Journal of Structural Geology 31 (2009) 601–614

Contents lists available at ScienceDirect

Journal of Structural Geology

journal homepage: www.elsevier.com/locate/jsg

Localisation of plastic flow in the mid-crust along a crustal-scale fault: Insight from the Hatagawa Fault Zone, NE Japan

Norio Shigematsu [a,*], Koichiro Fujimoto [b], Tomoyuki Ohtani [c], Bunichiro Shibazaki [d], Tomoaki Tomita [e,1], Hidemi Tanaka [f], Yukari Miyashita [a]

[a] Geological Survey of Japan, National Institute of Advanced Industrial Science and Technology, AIST Tsukuba Central 7, 1-1 Higashi, Tsukuba, Ibaraki 305-8567, Japan
[b] Faculty of Education, Tokyo Gakugei University, 4-1-1 NukuiKita-machi, Koganei, Tokyo 184-8501, Japan
[c] Department of Civil Engineering, Gifu University, 1-1 Yanagido, Gifu, Gifu 501-1193, Japan
[d] International Institute of Seismology and Earthquake Engineering, Building Research Institute, 1 Tatehara, Tsukuba, Ibaraki 305-0802, Japan
[e] Institute of Geoscience, The University of Tsukuba, 1-1-1 Tennodai, Tsukuba, Ibaraki 305-8571, Japan
[f] Department of Earth and Planetary Sciences, The University of Tokyo, 7-3-1 Hongo, Tokyo 113-0033, Japan

ARTICLE INFO

Article history:
Received 5 September 2008
Received in revised form
24 March 2009
Accepted 12 April 2009
Available online 19 April 2009

Keywords:
Fault zone
Brittle–plastic transition
Fault rocks
Heterogeneous plastic flow

ABSTRACT

This study examines plastic flow in fault rocks exposed along the Hatagawa Fault Zone (HFZ) of NE Japan. The fault zone, developed in 110 Ma granitoids, ceased activity by 98.1 ± 2.5 Ma. Three different fault rocks (mylonites with microstructures A and B, and cataclasite) are exposed along the fault. Microstructure A formed at the brittle–plastic transition. The temperature conditions for microstructure B were higher than those for microstructure A; those for the cataclasite were lowest. Microstructure A is exposed in limited areas (maximum length extent of approximately 6 km) along the HFZ. The distribution of microstructure A is considered to represent the latest-stage localised zones of plastic flow, associated with strain weakening accompanied by dynamic recrystallisation of feldspar, suggesting the restriction of plastic displacement to certain intervals at depth ranges with *P–T* conditions of the brittle–plastic transition. Many zones of localised deformation containing crush zones are observed in rocks with microstructure A, suggesting that numerous fractures nucleated due to the ductile fracturing of highly deformed fine-grained feldspar in the outcrop extent of microstructure A. The nucleation of large earthquakes was possibly promoted by interaction between fractures that nucleated by ductile fracture and stress concentrations associated with the restricted development of plastic displacement.

1. Introduction

The hypocentres of inland earthquakes are generally located in the shallow part of the Earth's crust, and mainshocks usually occur in the deepest part of the seismogenic zone (Sibson, 1982, 1984; Das and Scholz, 1983; USGS Staff, 1990; Nakamura and Ando, 1996). The temperature of the base of the seismogenic zone is between 300 and 400 °C (Ito, 1999), corresponding to the brittle–plastic transition in the Earth's crust (Sibson, 1982, 1984). These observations suggest the important role of plastic behaviour along the deep-level extensions of seismogenic faults in the generation of large inland earthquakes (Shimamoto, 1989; Scholz, 1990).

One possible nucleation mechanism of large inland earthquakes is interaction between the plastic behaviour of the deeper parts of crustal-scale fault zones and the frictional behaviour of shallower parts (Iio and Kobayashi, 2002; Shibazaki, 2002; Iio et al., 2004). To understand this interaction, it is necessary to determine the behaviours of fault zones around the base of the seismogenic zone (depth = 10–20 km), which presumably are located near the brittle–plastic transition; however, such regions are generally inaccessible along major active faults. Therefore, the investigation of exhumed crustal-scale fault zones for which deeper crustal sections (including the vicinity of the brittle–plastic transition) are exposed at the surface is an important strategy in understanding fault behaviour in such regions (e.g., Stewart et al., 2000).

Mixed brittle–plastic fault rocks reported along the Hatagawa Fault Zone (HFZ) of NE Japan (Takagi et al., 2000; Tomita et al., 2002; Shigematsu et al., 2004) represent an exhumed fault zone deformed in the vicinity of the brittle–plastic transition. In the present study, fault rocks were examined along the HFZ with the

* Corresponding author. Tel.: +81 29 861 3528; fax: +81 29 861 3682.
E-mail address: n.shigematsu@aist.go.jp (N. Shigematsu).
[1] Present address: FDC Incorporated Company, 111-2 Arakawaoki, Tsuchiura, Ibaraki 300-0873, Japan.

0191-8141/$ – see front matter © 2009 Elsevier Ltd. All rights reserved.
doi:10.1016/j.jsg.2009.04.004

aim of understanding fault behaviour around the base of the seismogenic zone.

2. Hatagawa Fault Zone

Two NNW–SSE-trending major crustal-scale faults are exposed at the eastern margin of the Abukuma Mountains, NE Japan. The western fault, the HFZ (Watanabe et al., 1953; Sendo, 1958) (Fig. 1), separates the Abukuma belt from the South Kitakami belt (Kubo and Yamamoto, 1990; Kubo et al., 1990). The Abukuma belt, which lies to the west of the HFZ, consists mainly of magnetite-free Cretaceous granitoids; the South Kitakami belt, which lies to the east, is dominated by magnetite-bearing Cretaceous granitoids. The HFZ contains three structural zones: a cataclasite zone of up to 100 m in width, mylonite zones with a sinistral sense of shear and a maximum width of >1 km, and small shear zones of less than 1 m in width (Takagi et al., 2000; Shigematsu and Yamagishi, 2002; Tomita et al., 2002) (Fig. 2). An undeformed granodiorite porphyry dike intruded into the cataclasite zone has been dated at 98.1 ± 2.5 Ma, indicating that major activity along the HFZ had ceased by this time (Tomita et al., 2002).

We studied a 45-km-long section along the HFZ (Fig. 1), focusing on the relationship between the cataclasite and mylonite zones.

3. Fault rocks within the HFZ

3.1. Mylonite zones with a sinistral sense of shear

Mylonite zones with a sinistral sense of shear are heterogeneously exposed along the entire 45 km length of the HFZ

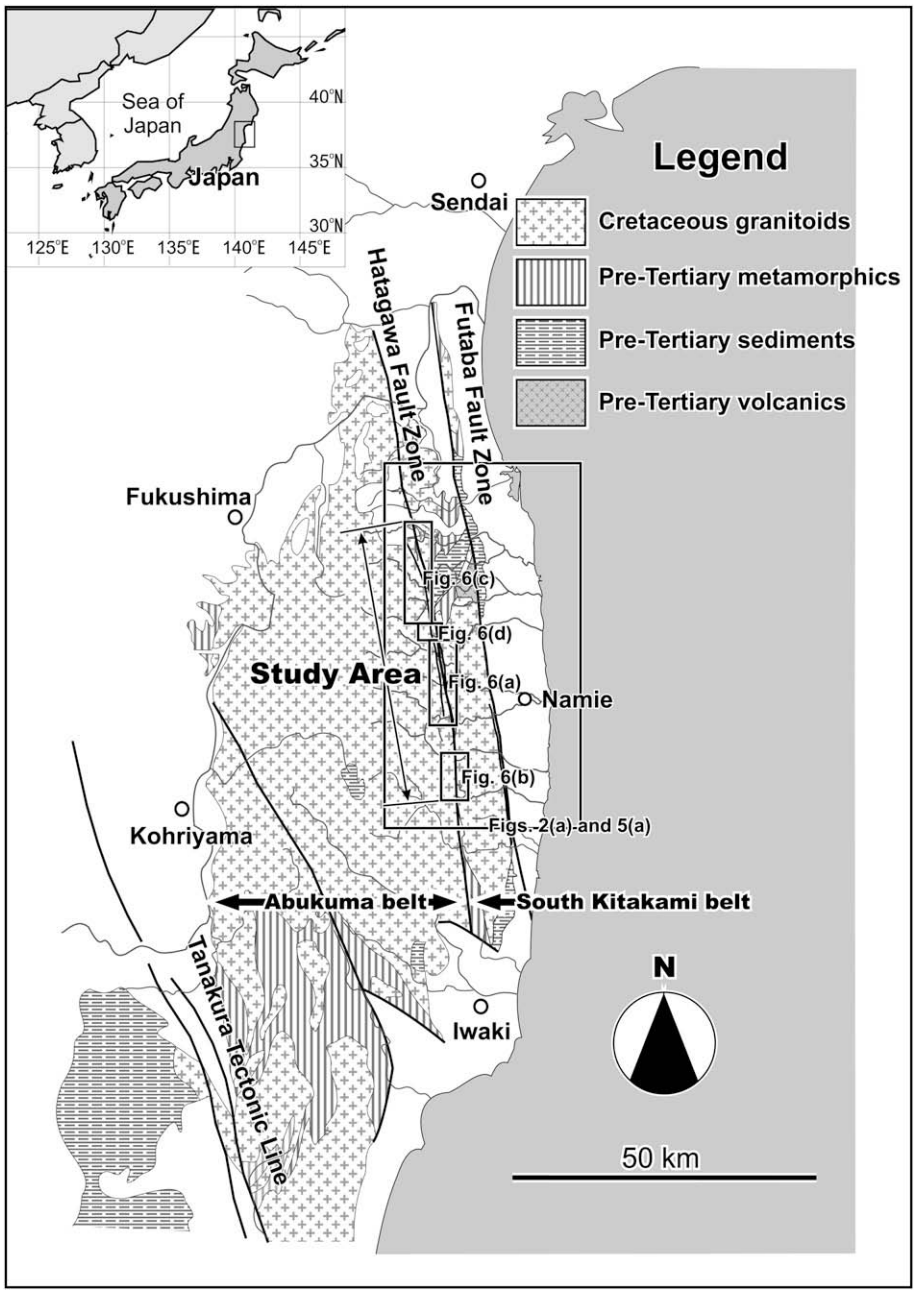

Fig. 1. Geological map showing the location of the study area, pre-Tertiary rocks, and major faults. The areas shown in Figs. 2a, 5a, and 6 are indicated by rectangles.

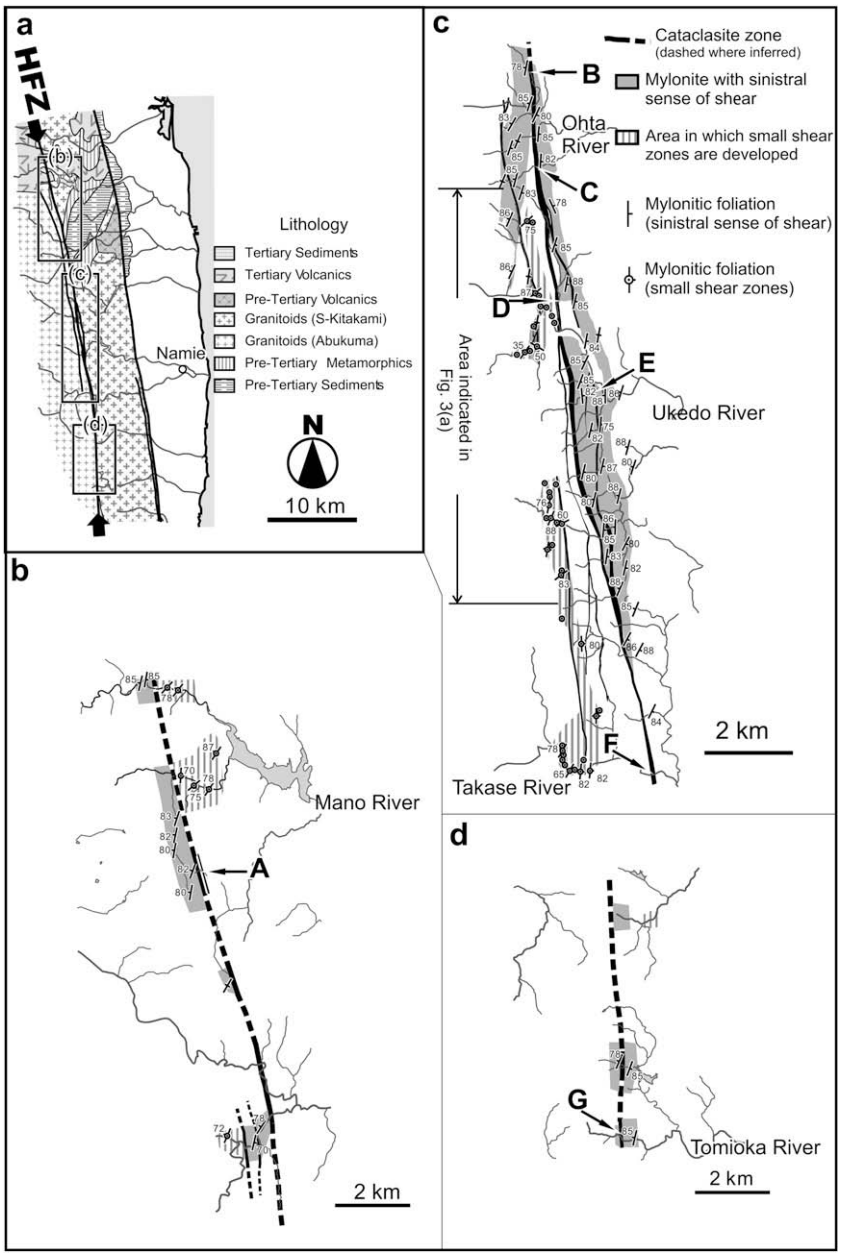

Fig. 2. Outcrop maps of fault rocks along the Hatagawa Fault Zone. (a) Summary geological map of the Abukuma Mountains, showing the locations of the maps presented in (b–d). Also shown are outcrop maps of fault rocks in the northern (b), central (c; modified from) Shigematsu et al., 2004, and southern (d) parts of the study area.

examined in this study (Fig. 2). These zones contain well-developed subvertical foliations that strike N–S and subhorizontal stretching lineations that trend N–S. The orientations of lineations near the Ukedo River are especially important in terms of the later discussion. Fig. 3 shows that lineations in mylonite near the Ukedo River are shallowly plunging, with consistent trends throughout the area. The lineations plunge gently to the north in the northern part of the area (Fig. 3b–d), and to the south in the southern part (Fig. 3e).

Shigematsu and Yamagishi (2002) identified two types of microstructures (A and B) along the HFZ, based solely on the microstructure of quartz; however, in the present paper we use this scheme to describe the general microstructures of the mylonites.

In microstructure A, quartz displays core–mantle structures (Fig. 4a) (White, 1976), whereby coarse ribbon grains (long axes of several hundred micrometres) are surrounded by fine grains (diameter <10 μm). The coarse ribbon grains are strongly flattened, with aspect ratios sometimes exceeding 20, and exhibit undulatory extinction, occasional deformation lamellae, and commonly contain well-developed subgrains. The fine quartz grains are equant in shape.

Shigematsu and Yamagishi (2002) reported that recrystallisation in microstructure A occurred predominantly by progressive subgrain rotation, based on optical and TEM observations; that is, the quartz was deformed under the conditions of regime 2 of Hirth and Tullis (1992). The lattice preferred orientations (LPOs) of quartz *c*-axes are characterised by type I crossed girdles (Shigematsu and Yamagishi, 2002). No myrmekite is observed associated with K-feldspar porphyroclasts, and feldspar porphyroclasts are commonly fractured (Fig. 4b). In strongly deformed mylonite with microstructure A, fine-grained feldspar layers are developed, with a typical grain size of approximately 1 μm (Fig. 4b and c). In such layers, fine plagioclase and K-feldspar grains are commonly

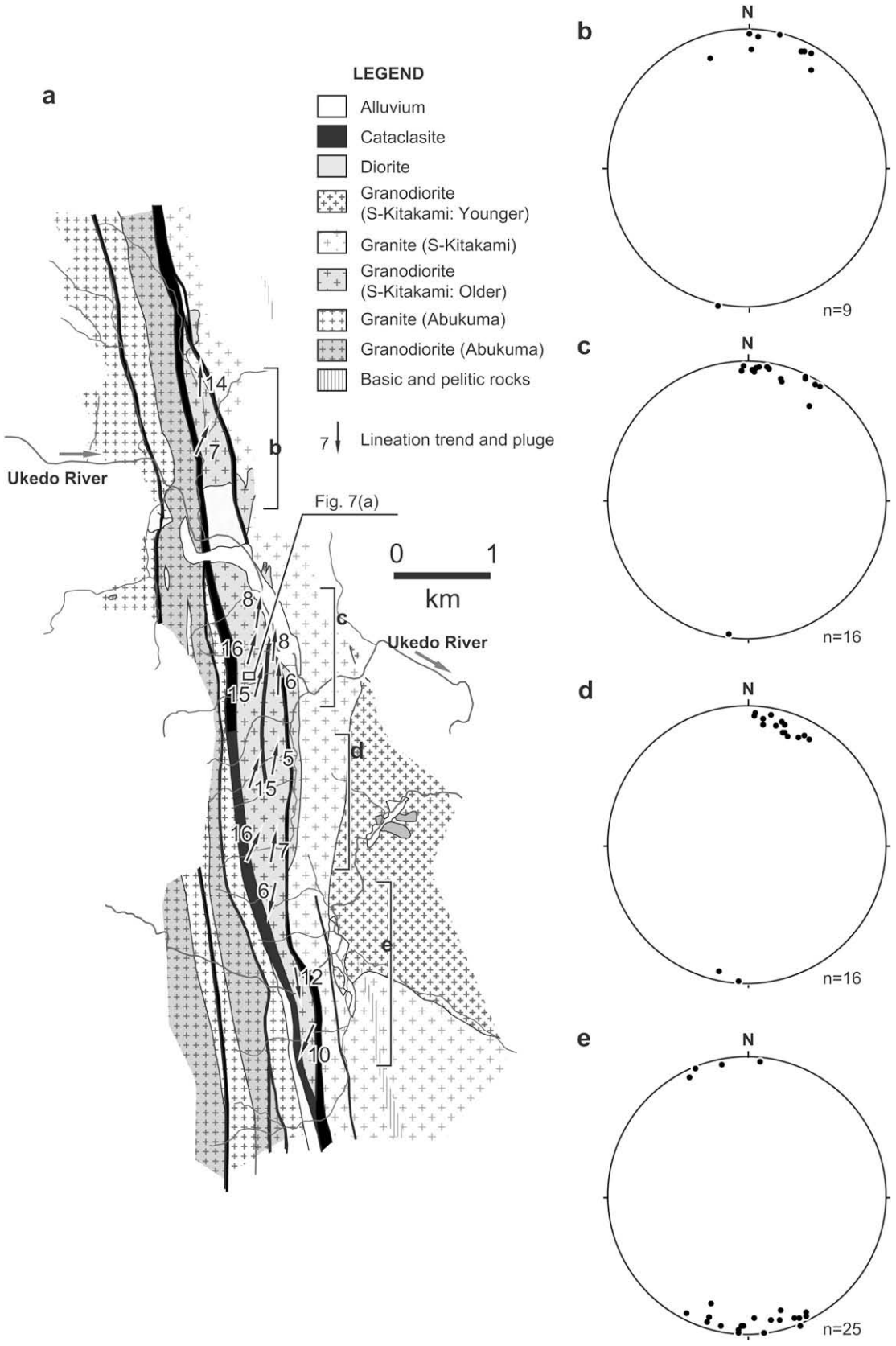

Fig. 3. Lineations in mylonite near the Ukedo River.(a) Geological map of the Ukedo River section. The rectangle indicates the location of Fig. 7a. (b–e) Stereoplots of lineation data from sub-areas in (a), arranged from north (b) to south (e). Lower hemisphere, equal-area projections.

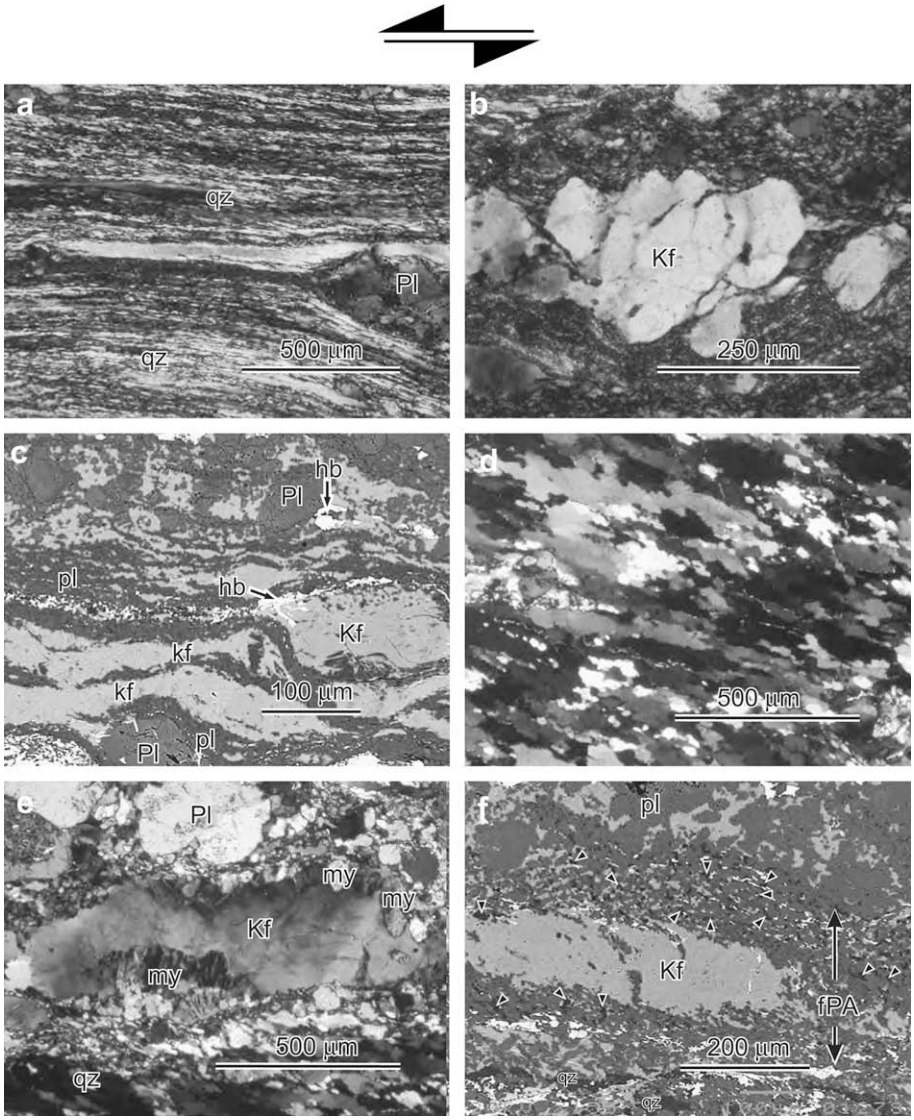

Fig. 4. Photomicrographs of microstructures within mylonites with a sinistral sense of shear, located along the Hatagawa Fault Zone. (a) Quartz (qz) microstructure within a mylonite with microstructure A (cross-polarised light). Pl: plagioclase porphyroclast. (b) K-feldspar porphyroclast (Kf) within a mylonite with microstructure A (cross-polarised light) (c) Back-scattered electron image of fine-grained feldspar within a mylonite with microstructure A. The contrast in the image enables different mineral phases to be distinguished. pl: fine-grained plagioclase; Pl: plagioclase porphyroclast; kf: fine-grained K-feldspar; Kf: K-feldspar porphyroclast; qz: quartz; hb: hornblende. (d) Quartz microstructure within a mylonite with microstructure B (cross-polarised light). (e) K-feldspar porphyroclast (Kf) surrounded by myrmekite (my) within a mylonite with microstructure B (cross-polarised light). Pl: Plagioclase porphyroclast; qz: quartz. (f) Back-scattered electron image of fine-grained polymineralic aggregate (fPA) within a mylonite with microstructure B. Kf: K-feldspar; pl: plagioclase; qz: quartz. Black arrowheads indicate fine-grained quartz within fPA. The arrows at the top of the figure indicate the sense of shear. The samples shown in (a)–(c) were collected at locality 1 in Fig. 5c. The samples shown in (d) and (e) were collected at locality 2 in Fig. 5c. The sample shown in (f) was collected at locality 3 in Fig. 5c.

clustered in aggregates with a shape preferred orientation parallel to the foliation (Fig. 4c). This type of microstructure has also been described in small shear zones along the HFZ, for which dynamic recrystallisation (Tullis and Yund, 1985, 1987) has been suggested as the deformation mechanism leading to its development (Shigematsu, 1999; Shigematsu and Tanaka, 2000).

In microstructure B, quartz grains have a smaller aspect ratio than those in microstructure A. The aspect ratio is invariable with grain size, and undulatory extinction is less strongly developed than in microstructure A (Fig. 4d). The minimum grain size of quartz is approximately 20 μm. Shigematsu and Yamagishi (2002) reported that recrystallisation in microstructure B occurred by both grain boundary migration and progressive subgrain rotation; that is, the quartz was deformed under the conditions of regime 3 of Hirth and Tullis (1992). The LPO patterns of quartz *c*-axes are characterised by a *Y*-maximum (Shigematsu and Yamagishi, 2002). K-feldspar porphyroclasts are replaced by myrmekite, a plagioclase–vermicular quartz symplectite (Simpson, 1985; Simpson and Wintsch, 1989; Vernon, 1992; Tsurumi et al., 2003; Ree et al., 2005) (Fig. 4e). Strongly deformed mylonite contains a fine-grained feldspar-dominated matrix (grain size, 10–20 μm) of fine-grained plagioclase, K-feldspar, and quartz (Fig. 4f) (Tsurumi et al., 2003).

Some samples show a microstructure intermediate between that of A and B (herein termed "intermediate microstructure"), in which quartz displays the features of microstructure A, yet feldspar shows features of microstructure B. In such rocks, myrmekite is well developed around K-feldspar porphyroclasts, and the matrix consists of fine-grained plagioclase, K-feldspar, and quartz.

Fig. 5 shows the regional distribution of microstructures A and B. Mylonite with microstructure B is exposed along the entire

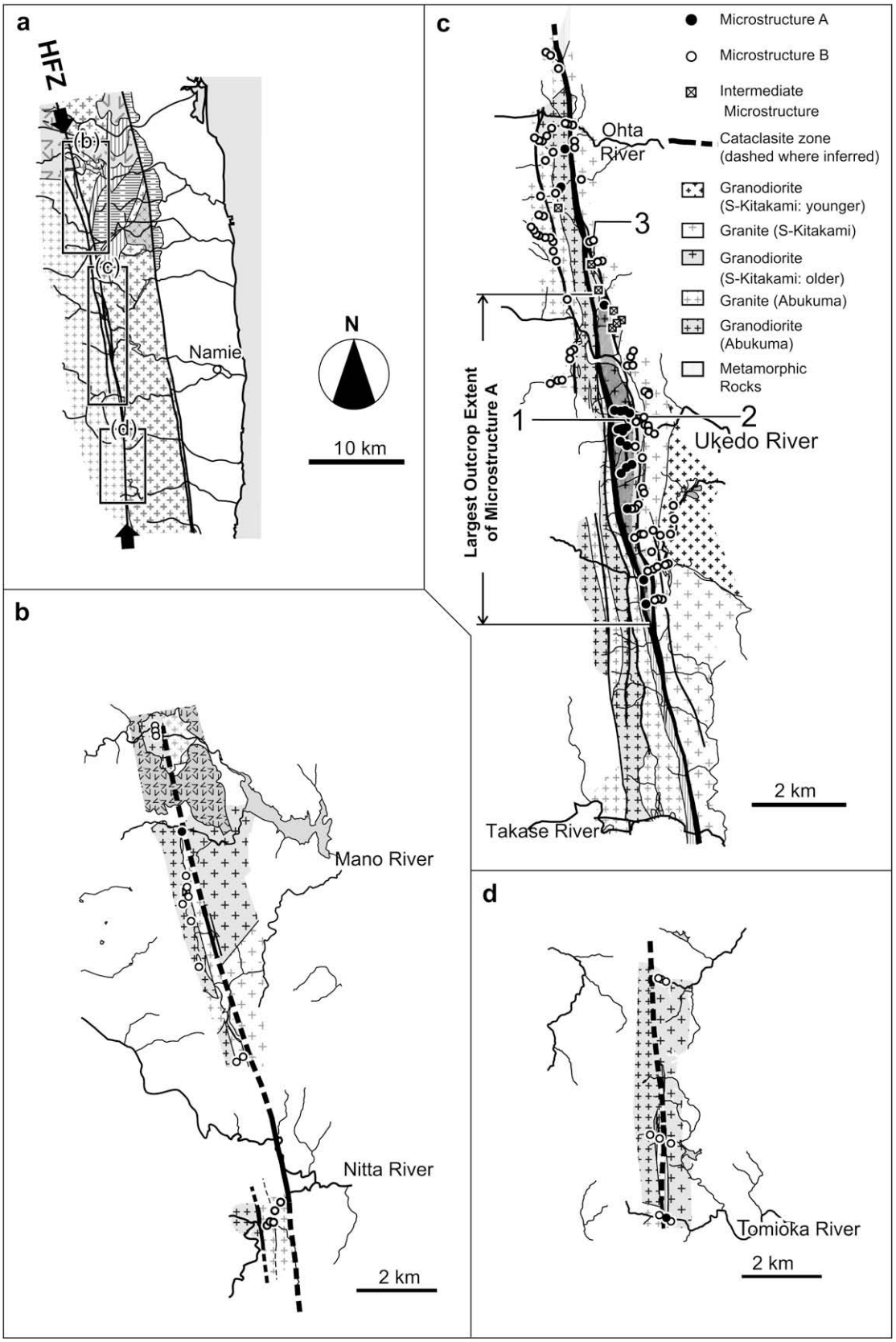

Fig. 5. Outcrop extent of mylonite microstructures. (a) Summary geological map of the Abukuma Mountains, showing the locations of geological maps (b–d) along the HFZ, which show the outcrop extent of microstructure A (solid circles), microstructure B (open circles), and the intermediate microstructure (open squares containing crosses) in the northern (b), central (c), and southern (d) parts of the study area. The shaded area in (c) indicates the largest outcrop extent of microstructure A.

45 km length of the examined HFZ, whereas mylonite with microstructure A is only locally exposed. The largest single outcrop of microstructure A extends for approximately 6 km along the HFZ (herein referred to as "largest outcrop extent of microstructure A"), with a width of 750 m, located to the east of the cataclasite zone near the Ukedo River (Fig. 5c). The eastern and northern margins of this largest outcrop extent of microstructure A (where a change in microstructure occurs) are located in older granodiorite of the South Kitakami belt. Microstructure A is also observed west of the cataclasite zone near the Ohta River (Fig. 5c), east of the cataclasite zone near the Tomioka River (Fig. 5d), and at a locality in the northern part of the study area (Fig. 5b).

The compositions of fine-grained K-feldspar (orthoclase) and adjacent plagioclase were analysed using an electron probe microanalyser (EPMA; JEOL JXA 8800R housed at the Geological Survey of Japan, AIST, Japan) to constrain the syn-deformation temperature. The mole fractions of Na in orthoclase are shown in Fig. 6. The mole fraction of Na in orthoclase within microstructure A ranges from 1.7% to 3.47%, whereas values exceeding 5% are found in the samples with microstructure B and intermediate microstructure, although the compositions are widely variable. Microstructure B and the intermediate microstructure yield similar mole fractions of Na in orthoclase.

Many zones of localised deformation are heterogeneously distributed throughout the largest outcrop extent of microstructure A (Fig. 7). The exposure shown in Fig. 7a lies on a slope dipping at 45° to the N; the figure represents a projection into the horizontal surface of the intersection between the zones of localised deformation and the slope. The zones of localised deformation generally contain dark-coloured ultramylonite zones; in places, weakly deformed protomylonite changes into strongly deformed ultramylonite over a distance of just several centimetres (Fig. 7b).

The width of the zones of localised deformation is variable, ranging from several millimetres to several tens of centimetres (Fig. 7a). The lengths of narrow localised zones are generally shorter than those of wide zones: those zones of localised deformation narrower than 1 cm extend for only several metres, whereas those wider than several centimetres continue for more than several tens of metres, commonly beyond the limits of the exposure.

Ultramylonites within the dark-coloured ultramylonite zones are commonly cataclastically fragmented, forming crush zones (Fig. 7b and c). The crush zones are only developed in the dark-coloured ultramylonite zones, and are oriented parallel to the trend of the zones of localised deformation. In some samples, the foliation in rock fragments is dragged in the direction of the sense of shear recorded in adjacent ultramylonite zones (arrow in Fig. 7d).

3.2. Cataclasite zone

A conspicuous cataclasite zone with a maximum width of 100 m extends continuously for at least 40 km along the HFZ (Fig. 2). The cataclasite consists of fragments of mylonite, undeformed granitoids, and pseudotachylyte (Figs. 8 and 9) within a matrix of chlorite, epidote, and calcite, but not montmorillonite, indicating that the cataclasite zone formed at temperatures above 220 °C (Tomita et al., 2002). This interpretation is based on the fact that in active geothermal fields, epidote and chlorite are stable at temperatures above 200 °C, and montmorillonite is stable below 220 °C (Henley and Ellis, 1983).

The sample from locality E shown in Fig. 2c contains pseudotachylyte developed in cataclasite (Fig. 8). Fragments in this cataclasite are in permanent extinction under cross-polarised light (Fig. 8b and c), suggesting an amorphous structure such as that of glass; i.e., the fragments were originally pseudotachylyte, and there occurred repeated earthquakes along the cataclasite zone, without plastic deformation.

The microstructure of fragments in the cataclasite zone changes along the strike of the HFZ. Most of the fragments consist of undeformed granitoids at exposures A, B, and F shown in Fig. 2b and c. The microstructure at exposure B is shown in Fig. 9a and b. The cataclasites at exposures C and G shown in Fig. 2c and d contain fragments of mylonite and undeformed granitoids. The microstructure at exposure C is shown in Fig. 9c and d. Most of the fragments at exposure D shown in Fig. 2c, where the exposure is adjacent to the largest outcrop extent of microstructure A (see also Fig. 5c), consist of mylonite (Fig. 9e and f).

In quartz fragments within cataclasite at exposure D, very fine grains (diameter $<10\,\mu m$) occur along the boundaries of larger grains (Fig. 9h), whereas at exposure C the sizes of such grains are several tens of micrometres (Fig. 9g). This observation, together with the relatively intensive development of undulatory extinction at exposure D (Fig. 9h), suggests that the quartz microstructure in fragments of cataclasite at exposure D is microstructure A, while that at exposure C is microstructure B. The shape preferred orientation does not help to identify the type of microstructure in fragments of cataclasite, as the fragments themselves are randomly oriented.

4. Discussion

4.1. Deformation conditions of fault rocks along the HFZ

It has been suggested that the various types of fault rocks along the HFZ were deformed under different temperature conditions. In considering microstructure A, Shigematsu and Yamagishi (2002) suggested that quartz was deformed in regime 2 dislocation creep (see Hirth and Tullis, 1992), and reported that the LPO of *c*-axes shows a type I crossed girdle. For microstructure B, the authors suggested that quartz was deformed in regime 3 dislocation creep (Hirth and Tullis, 1992), and in this case the LPO of *c*-axes typically shows a *Y*-maximum.

The mole fractions of Na in fine-grained orthoclase (Fig. 6) suggest a difference in syn-deformation temperature between microstructures A and B. The following findings suggest that the chemical composition of fine-grained feldspar grains changed during deformation. Observations by transmission electron microscopy (TEM) (Shigematsu, 1999; Shigematsu and Tanaka, 2000) suggest that the fine grains in microstructure A formed by dynamic recrystallisation. During this process, feldspar composition can change via both grain boundary diffusion and migration processes (Yund and Tullis, 1991). In such a case, the migration of a grain boundary by 1 μm (the size of feldspar grains) would change the composition of feldspar grains, resulting in a more rapid change in composition than that expected for diffusion-dominated processes. Observations of microstructure B (Tsurumi et al., 2003) suggest that feldspar composition changed via the syn-deformation myrmekite-forming reaction (Simpson and Wintsch, 1989; Tsurumi et al., 2003).

The equilibrium composition of orthoclase is constrained by the solvus curve in the $NaAlSi_3O_8$–$KAlSi_3O_8$ system (e.g., Yund and Tullis, 1983; Brown and Parsons, 1989), and a smaller mole fraction of Na in orthoclase is expected at lower equilibrium temperatures. Alkali ions have high diffusion coefficients (Yund, 1983; Christoffersen et al., 1983), and Na–K exchange between orthoclase and plagioclase can occur even under lower temperatures; therefore, in the present case some of the mole fraction of Na in orthoclase might have been reduced during cooling of the granitic bodies after attaining an equilibrium composition at the syn-deformation temperature.

Fine-grained orthoclase grains in microstructure B and the intermediate microstructure contain more Na than do grains in

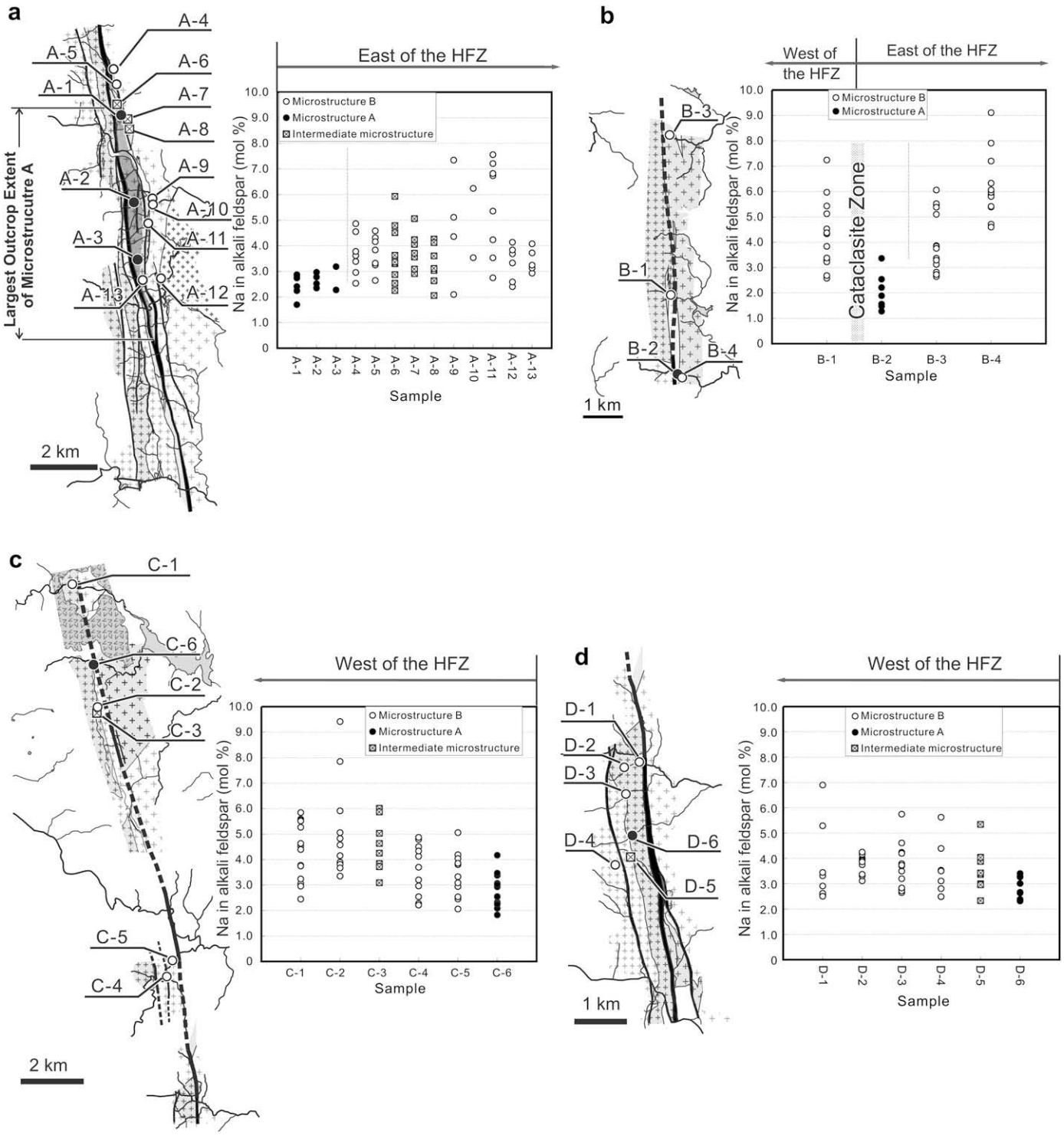

Fig. 6. Mole fraction of Na in fine-grained orthoclase in the mylonite with a sinistral sense of shear along the HFZ. The locations of the maps are shown in Fig. 1. The shaded area in the map shown in (a) indicates the largest outcrop extent of microstructure A.

microstructure A (Fig. 6). This observation, together with the difference in microstructure between microstructures A and B (Fig. 4) (Shigematsu and Yamagishi, 2002), suggests that the syn-deformation temperature of microstructure B was higher than that of microstructure A. The wide variety of mole fractions of Na in orthoclase may reflect the cooling of granitic bodies after deformation. The largest mole fractions of Na in fine-grained orthoclase within sample A-3 (see Fig. 6a), combined with the composition of adjacent plagioclase grains, yield a temperature of 346 °C using a two-feldspar geothermometer (Whitney and Stormer, 1977), assuming the measured feldspar compositions were in equilibrium at a pressure of 300 MPa. A comparable analysis of sample A-6 (see Fig. 6) yields a temperature of 40 °C.

Several features within the outcrop extent of microstructure A suggest an association between fracturing and plastic deformation (Fig. 7). Many zones of localised deformation contain dark-coloured

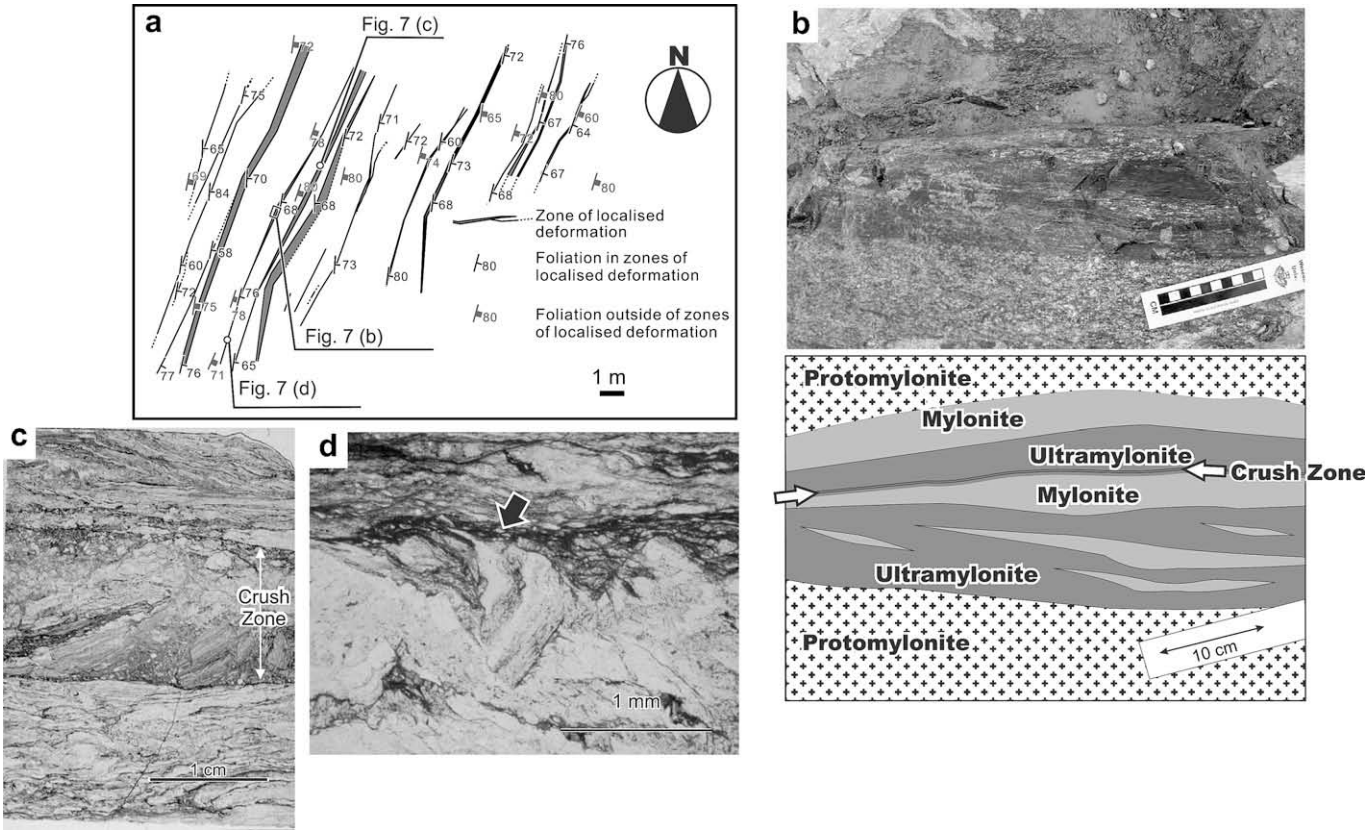

Fig. 7. Photomicrographs showing the relationship between plastic deformation and fracturing. (a) Zones of localised deformation within the largest outcrop extent of microstructure A. The location of the outcrop is indicated in Fig. 3a. Also indicated are the locations of (b–d). (b) Zone of localised deformation. (c) Microstructure of a zone of localised deformation. Note the fragmentation of mylonite in the centre of the zone of localised deformation. (d) Microstructure of another zone of localised deformation (modified from Tomita et al., 2002). Along the boundary of this zone (arrow), the foliation in rock fragments has been dragged in the direction of the sense of shear.

ultramylonite zones, which in turn contain crush zones (Fig. 7a–c) oriented parallel to the trend of the zones of localised deformation. In some samples, the foliation in fragments is dragged in the direction of the sense of shear recorded in adjacent ultramylonite zones (Fig. 7d). These structures are similar to those reported previously in a small shear zone along the HFZ that shows evidence of repeated fracturing and plastic deformation (Shigematsu et al., 2004). These observations suggest that the deformation conditions leading to microstructure A were close to those of the brittle–plastic transition. Although the matrix minerals in cataclasite suggest deformation at temperatures above 220 °C (Tomita et al., 2002), the cataclasite zone was deformed within the brittle/cataclastic regime, at temperatures lower than those at the brittle–plastic transition.

4.2. Limited outcrop extent of microstructure A

The outcrop extent of microstructure A is largely limited to a length of approximately 6 km along the strike of the HFZ (Figs. 5b and 6a). The microstructures of fragments in cataclasite (Fig. 9) suggest that the outcrop of microstructure A did not originally extend along the entire length of the fault zone. Most of the fragments consist of undeformed granitoids exposed *in situ* in outcrops located far from the largest outcrop extent of microstructure A (A, B, and F in Fig. 2; see also Fig. 9a and b). In contrast, most of the fragments in the exposure located next to the largest outcrop extent of microstructure A (D in Fig. 2; see also Fig. 9e and f) consist of mylonite that shows microstructure A (Fig. 9h). It is therefore unlikely that some of the rocks bearing microstructure A were obscured beyond recognition by the overprinting effects of later cataclasis.

Two possibilities can account for the outcrop extent of microstructure A: (1) plastic flow was localised during cooling of the granitic bodies, with the outcrop extent of microstructure A corresponding to the latest-stage localised zones of plastic flow at low temperatures; or (2) contrasting exhumation levels arising from late-stage tectonic movements. We believe that the former possibility is more likely than the latter. In a study of a mylonite with microstructure B along the HFZ, Tsurumi et al. (2003) demonstrated changing deformation conditions with progressive strain localisation (i.e., the localisation of plastic flow during cooling of the granitic bodies), based on an analysis of quartz *c*-axis fabrics and the composition of fine-grained feldspar.

In terms of the latter possibility, the occurrence of microstructure A would correspond to a basin or a downthrown block, thereby requiring the existence of structures responsible for the differences in the present-day exhumation level. The largest outcrop extent of microstructure A is surrounded by cataclasite zones (Fig. 5c); however, the eastern and northern margins of this outcrop extent are located in older granodiorite of the South Kitakami belt, indicating that the cataclasite zones do not control the outcrop extent. It is also unlikely that other, as yet unidentified, structures controlled the varying levels of exhumation, as the plunges of lineations are largely consistent throughout the largest outcrop extent of microstructure A (Fig. 3), and we have not found any young faults that cut the HFZ.

Although K–Ar ages can be used to constrain the exhumation level rate based on the contrasting closure temperatures of

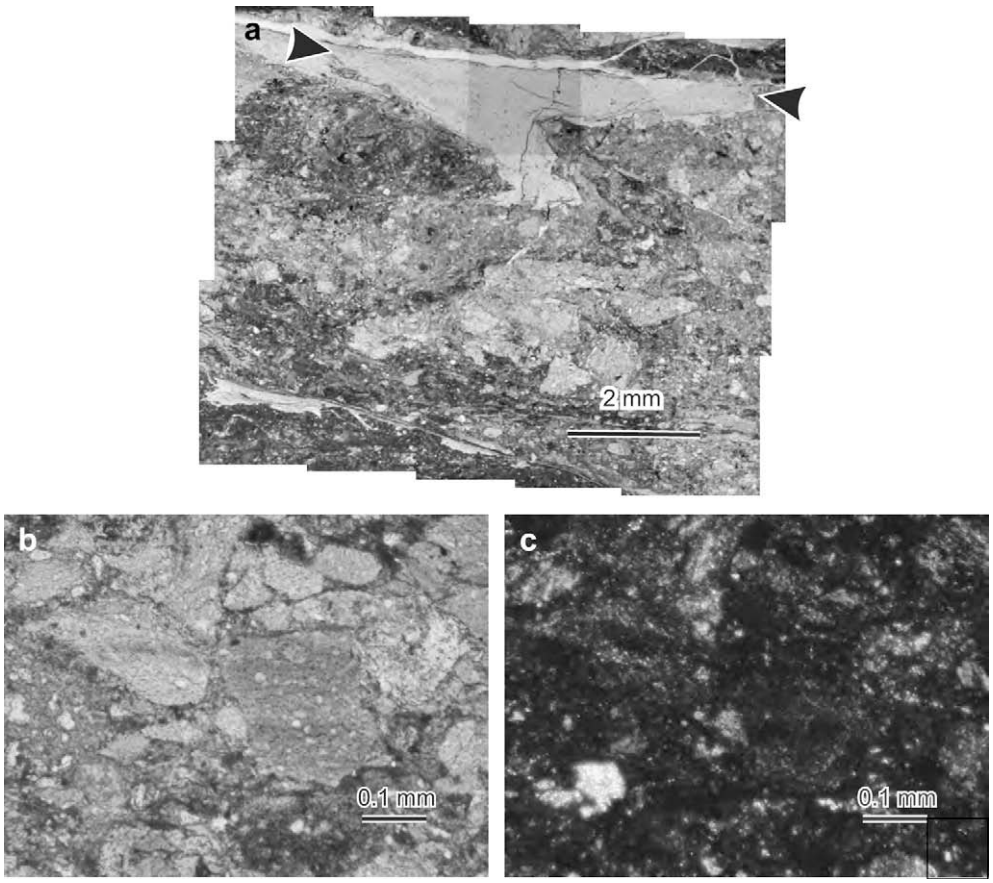

Fig. 8. Example of cataclastic microstructure containing a pseudotachylyte vein. The sampling locality is locality E shown in Fig. 2c. (a) Pseudotachylyte vein (arrows) developed in cataclasite. (b, c) Rock fragments in the same cataclasite as that shown in (a). (b) Plane-polarised light. (c) Cross-polarised light. Note that the fragments are extinct under cross-polarised light, suggesting they were originally pseudotachylyte and indicating several stages of pseudotachylyte formation.

hornblende and biotite (Dodson and McClelland-Brown, 1985), K–Ar ages reported for hornblende and biotite along the HFZ all cluster around 110 Ma (Kubo and Yamamoto, 1990; Kubo et al., 1990; Tomita et al., 2002; Ohtani et al., 2004). These ages indicate that the cooling rate of the granitic bodies was too rapid (relative to the errors in K–Ar ages) to enable the exhumation rate to be determined.

Given the above observations, the history of the HFZ at the present-day exhumation level can be summarised in terms of the following four stages. (1) Plastically deformed mylonite with microstructure B formed along almost the entire length of the HFZ (shaded area in Fig. 10a). Activity within the HFZ started at approximately 110 Ma, just after the emplacement of granitic intrusions. (2) During cooling of the granitic bodies, *P*–*T* conditions approached those of the brittle–plastic transition. Plastic flow became highly localised, restricted to the narrow present-day areas of microstructure A (shaded area in Fig. 10b). During this stage, those rocks showing microstructure A experienced alternating periods of plastic flow and fracturing. (3) The deformation conditions subsequently changed, with the present-day exhumation level deformed by brittle/cataclastic processes at temperatures above 220 °C (at lower temperatures than those for microstructure A); accompanying seismic activity is indicated by the generation of pseudotachylyte (Fig. 8). Cataclasite formed along almost the entire length of the HFZ (solid lines in Fig. 10c). (4) Finally, tectonic activity ceased by 98.1 ± 2.5 Ma (intrusion age of undeformed granodiorite porphyry dikes) (Tomita et al., 2002).

4.3. Implications of localised plastic flow for the generation of large earthquakes

The outcrop extent of fault rocks in the present case represents a schematic cross-section of deformation styles along the HFZ (Fig. 10d). In the depth range for which the *P*–*T* conditions corresponded to the brittle–plastic transition, the fault was partitioned into sections undergoing plastic flow (the present-day extent of microstructure A) and those not undergoing plastic flow. In contrast, displacement along the fault occurred along almost its entire length in the depth ranges for which rocks were subjected to plastic flow recorded by microstructure B, or brittle deformation. To accommodate the compatibility of displacement along the fault, displacement via brittle/cataclastic processes must have occurred along those sections not affected by plastic flow in the depth range for which the *P*–*T* conditions corresponded to the brittle–plastic transition.

The localisation of plastic flow during cooling of the granitic bodies has been reported previously in a study of a mylonite with microstructure B along the HFZ (Tsurumi et al., 2003). Such localised flow probably continued after the deformation conditions had changed to those that resulted in the formation of microstructure A. Further localisation of deformation in the outcrop extent of microstructure A was possibly due to strain weakening accompanied by dynamic recrystallisation of feldspar (Tullis and Yund, 1985; Rutter, 1999), which is commonly observed within zones of localised deformation developed in the outcrop extent of microstructure A (Fig. 4b and c; see also Fig. 7) (Shigematsu, 1999; Shigematsu and

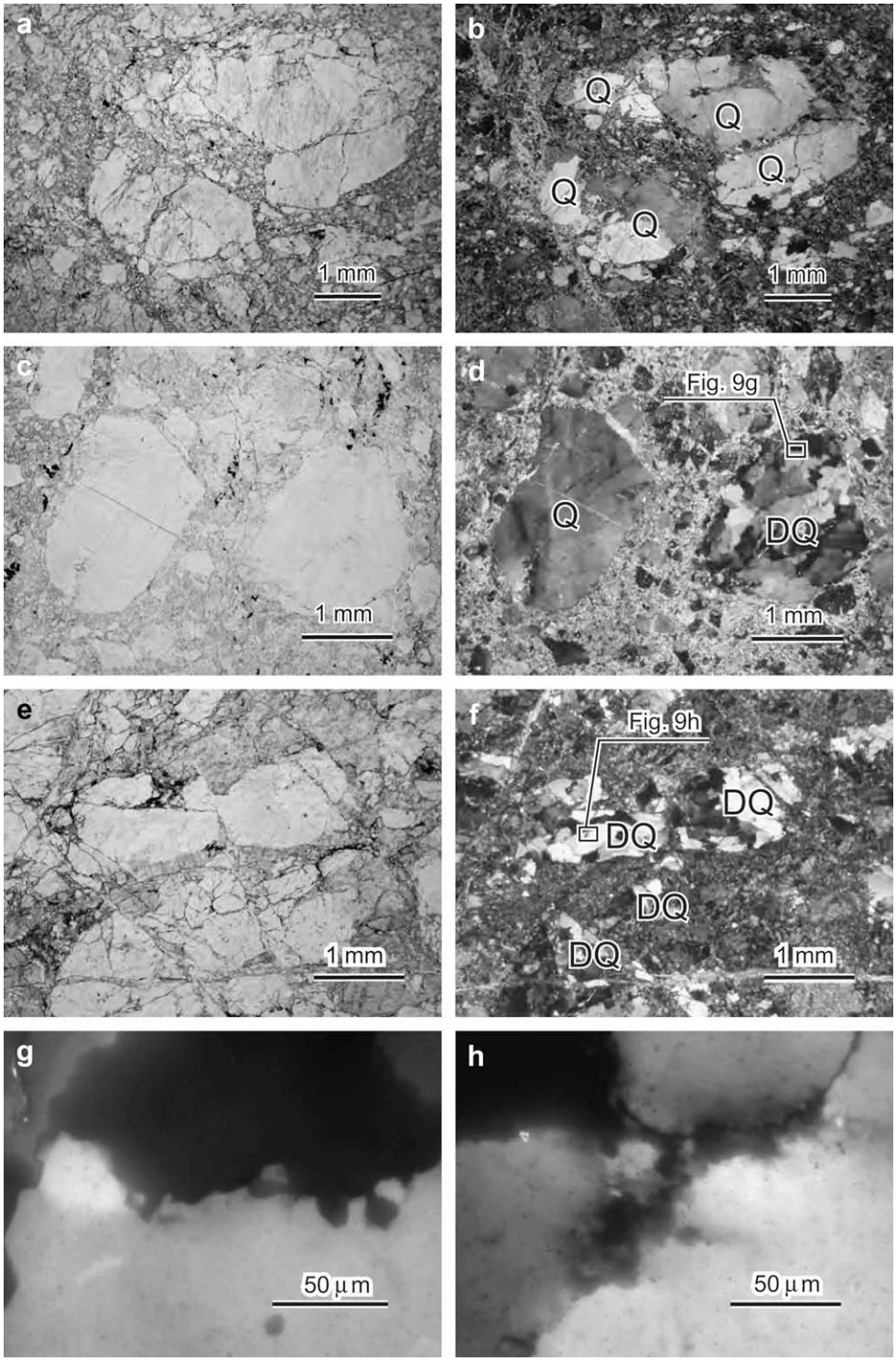

Fig. 9. Examples of cataclastic microstructure along the Hatagawa Fault Zone. The sampling localities are indicated in Fig. 2. (b, c) Microstructure of cataclasite at exposure B in Fig. 2c, in which most of the fragments are undeformed granitoids. (c, d) Microstructure of cataclasite at exposure C shown in Fig. 2c, which contains fragments of mylonite and undeformed granitoids. (e, f) Microstructure of cataclasite at locality D shown in Fig. 2c. Most of the fragments are mylonite. (g,h) Detailed quartz microstructures in fragments of cataclasite at exposures C and D, respectively. The positions of (g) and (h) are indicated in (d) and (f), respectively. (a), (c), and (e): Plane-polarised light. (b), (d), (f), (g), and (h): Cross-polarised light. The fragments labelled Q in (b), (d), and (f) are undeformed quartz; those labelled DQ are dynamically recrystallised quartz.

Tanaka, 2000). For this deformation mechanism, once the critical strain necessary for the onset of strain weakening is attained, localised plastic flow can develop spontaneously (Rutter, 1999). This mechanism may have resulted in the development of numerous zones of localised deformation (Fig. 7).

Crush zones are commonly developed within zones of localised deformation in the outcrop extent of microstructure A (Fig. 7). Shigematsu et al. (2004) suggested that similar structures found in a small shear zone within the HFZ formed via ductile fracturing of highly deformed fine-grained feldspar, as recently confirmed

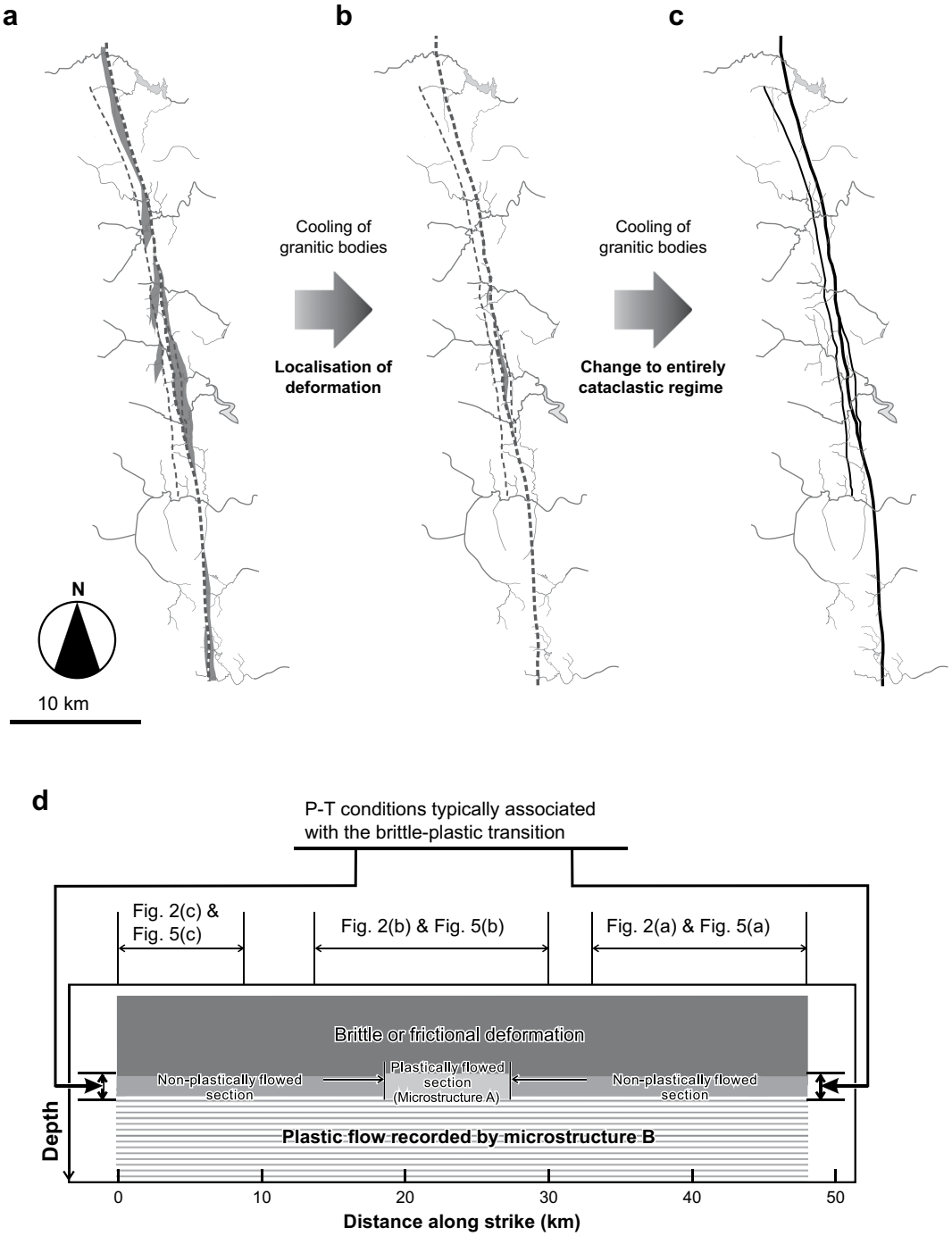

Fig. 10. (a–c) History of the Hatagawa Fault Zone (HFZ) at the present-day exhumation level. (a) Shading indicates areas that underwent plastic flow when the present-day exhumation level was subjected to deformation and metamorphic conditions favouring fully plastic mylonite-forming deformation (microstructure B). Dashed lines indicate present-day cataclasite zones. (b) Following the cooling of nearby granitic bodies, plastic deformation became highly localised at the *P–T* conditions of the brittle–plastic transition. Shading indicates the areas that underwent plastic flow when the present-day exhumation level was subjected to *P–T* conditions of the brittle–plastic transition (outcrop extent of microstructure A). Dashed lines indicate present-day cataclasite zones. (c) Further cooling of nearby granitic bodies led to a change in deformation conditions to brittle/cataclastic deformation. Solid lines indicate brittle/cataclastic deformation that occurred at temperatures above 220 °C. (d) Schematic cross-section showing the deformation styles along the active HFZ, as estimated from the outcrop extent of various fault rocks (Fig. 5). Also shown are the locations of the areas presented in Figs. 2 and 5.

experimentally (Rybacki et al., 2008). It is likely that many fractures nucleated via the ductile fracturing that accompanied extreme strain localisation in the outcrop extent of microstructure A.

Within the HFZ, plastic displacement was restricted to regions in the depth range of crust that experienced *P–T* conditions of the brittle–plastic transition (Fig. 10d). Such heterogeneity of displacement is likely to have resulted in a significant stress concentration in surrounding regions undergoing plastic flow, possibly leading to the nucleation of large earthquakes (e.g., Shibazaki et al., 2004). It is also possible that large earthquakes nucleated as a result of interaction between fractures that nucleated by ductile fracturing within plastically flowing regions (Fig. 7) and stress concentrations due to heterogeneous plastic displacement.

The localisation of plastic flow at the base of the seismogenic zone seems to have played an important role in the nucleation of large earthquakes in the HFZ; however, several problems remain to

be explained. For example, the limited outcrop extent of microstructure A suggests that the large strain necessary for the onset of strain weakening was only attained within restricted regions at the *P–T* conditions of the brittle–plastic transition. One possible explanation in this regard is the heterogeneous nature of the plastic displacement recorded by microstructure B along the HFZ, and that the large strain required to initiate strain localisation at the *P–T* conditions of the brittle–plastic transition was simply inherited from the large plastic strain recorded by microstructure B. The mylonite zone near the Ukedo River (Fig. 2b) (close to the largest outcrop extent of microstructure A) is more than 1 km wide, whereas that in the northernmost part of the study area (Fig. 2a) is just several hundred metres wide, suggesting the heterogeneity of plastic displacement recorded by microstructure B. This heterogeneity could have resulted from the intrusion of a younger granodioritic rock body east of the largest outcrop extent of microstructure A (Figs. 3a and 5c) (Kubo and Yamamoto, 1990: Kubo et al., 1990).

With regard to the above findings, few studies have reported comparable heterogeneity along other exhumed crustal-scale fault zones. Furthermore, it is unclear whether the findings of the present study are consistent with geophysical observations. For example, many large inland earthquakes appear to occur in areas with a steep gradient in the depth of the base of the seismogenic zone (Ito, 1999). Some hypocentres of the mainshocks of inland earthquakes are located in zones with distinctive P- and S-wave velocities and Poisson's ratio (Zhao and Negishi, 1997). Accordingly, additional research is necessary to improve our understanding of fault behaviour around the base of the seismogenic zone.

5. Conclusions

We documented the occurrences of fault rocks along the Hatagawa Fault Zone (HFZ) of NE Japan, with the aim of understanding the behaviour of faults around the base of the seismogenic zone. We draw the following conclusions based on the obtained results.

(1) Three different fault rocks (mylonites with microstructures A and B, and cataclasite) are exposed along the HFZ. The microstructures of these rocks and the chemical composition of fine-grained feldspar indicate that deformation conditions leading to the formation of microstructure A were close to those of the brittle–plastic transition. The syn-deformation temperatures estimated for mylonite with microstructure B are higher than those of the brittle–plastic transition, whereas the temperatures estimated for cataclasite are lower.
(2) Microstructure A occurs in limited regions along the HFZ, along a maximum length of approximately 6 km. This outcrop extent of microstructure A is considered to represent the final localised zone of plastic flow within the HFZ. Displacement by plastic flow occurred only in restricted regions at the depth in the crust where *P–T* conditions were equal to those of the brittle–plastic transition.
(3) The localisation of deformation to the outcrop extent of microstructure A possibly resulted from strain weakening accompanied by the dynamic recrystallisation of feldspar. This mechanism also resulted in the development of numerous zones of localised deformation.
(4) Many zones of localised deformation (also containing crush zones) developed within the outcrop extent of microstructure A, suggesting that the extreme strain localisation led to ductile fracturing of highly deformed fine-grained feldspar. It is likely that numerous fractures nucleated in these rocks due to ductile fracture.
(5) The occurrence of plastic displacement in the restricted regions of crust for which the *P–T* conditions approached those of the brittle–plastic transition resulted in a significant stress concentration. Interaction between this stress concentration and fractures nucleated via ductile fracture possibly promoted the nucleation of large earthquakes.

Acknowledgements

The authors sincerely thank Drs. Y. Kuwahara, K. Imanishi, Y. Iio, K. Kanagawa, T. Nakajima and M. Fukuyama for valuable discussions. This work was funded by Special Coordination Funds for Promoting Science and Technology, provided by the Ministry of Education, Culture, Sports, Science and Technology of Japan (Comprehensive Research Program on Flow and Slip Processes In and Below the Seismogenic Region). We also appreciate Dr. Kyuichi Kanagawa and an anonymous reviewer for their assistance in improving an early draft of the manuscript.

References

Brown, W.L., Parsons, I., 1989. Alkali feldspars: ordering rates, phase transformations and behavior diagrams for igneous rocks. Mineralogical Magazine 53, 25–42.
Christoffersen, R., Yund, R.A., Tullis, J., 1983. Inter-diffusion of K and Na in alkali feldspars: diffusion couple experiments. American Mineralogist 68, 1126–1133.
Das, S., Scholz, C.H., 1983. Why large earthquakes do not nucleate at shallow depth. Nature 305, 621–623.
Dodson, M.H., McClelland-Brown, E., 1985. In: Isotopic and paleomagnetic evidence for rates of cooling, uplift and erosion. Geological Society, London, Memoirs, pp. 315–320. 10.
Henley, R.W., Ellis, A.J., 1983. Geothermal systems ancient and modern: a geochemical review. Earth-Science Reviews 19, 1–50.
Hirth, G., Tullis, J., 1992. Dislocation creep regimes in quartz aggregates. Journal of Structural Geology 14, 145–159.
Iio, Y., Kobayashi, Y., 2002. A physical understanding of large intraplate earthquakes. Earth Planets Space 54, 1001–1004.
Iio, Y., Sagiya, T., Kobayashi, Y., 2004. What controls the occurrence of shallow intraplate earthquakes? Earth Planets Space 56, 1077–1086.
Ito, K., 1999. Seismogenic layer, reflective lower crust, surface heat flow and large inland earthquakes. Tectonophysics 306, 423–433.
Kubo, K., Yamamoto, T., 1990. Cretaceous intrusive rocks of Haramachi district, eastern margin of Abukuma mountains: Petrography and K–Ar age. Journal of Geological Society Japan 96, 731–743 (in Japanese with English abstract).
Kubo, K., Yanagisawa, Y., Yoshioka, T., Yamamoto, T., Takizawa, F., 1990. Geology of the Haramachi and Omika district with Geological Sheet Map at 1:50,000. Geological Survey of Japan, Tsukuba 155 pp (in Japanese with English abstract).
Nakamura, M., Ando, M., 1996. Aftershock distribution of the January 17, 1995 Hyogo-ken Nanbu earthquake determined by the JHD method. Journal of Physics of the Earth 33, 329–335.
Ohtani, T., Shigematsu, N., Fujimoto, K., Tomita, T., Iwano, H., 2004. Geochronological constraint on the brittle-plastic deformation along the Hatagawa Fault Zone, NE Japan. Earth Planets Space 56, 1201–1207.
Ree, J.-H., Kim, H.S., Han, R., Jung, H., 2005. Grain-size reduction of feldspars by fracturing and neocrystallization in a low-grade granitic mylonite and its rheological effect. Tectonophysics 407, 227–237.
Rutter, E.H., 1999. On the relationship between the formation of shear zones and the form of the flow law for rocks undergoing dynamic recrystallizatisation. Tectonophysics 303, 147–158.
Rybacki, E., Wirth, R., Dresen, G., 2008. High-strain creep of feldspar rocks: Implication for cavitation and ductile failure in the lower crust. Geophysical Research Letters 35, L04303. doi:10.1029/2007GL032478.
Scholz, C.H., 1990. The Mechanics of Earthquakes and Faulting. Cambridge University Press, Cambridge.
Sendo, T., 1958. On the granitic rocks of Mt. Otakine and its adjacent districts in Abukuma massif, Japan. Science Report of the Tohoku University Third Series 6. 57-167.
Shibazaki, B., 2002. Nucleation of large earthquakes determined by the seismic-aseismic boundary: Agreement between models and observations. Physics of the Earth and Planetary Interiors 134, 129–138.
Shibazaki, B., Shigematsu, N., Tanaka, H., 2004. Modelling slips and their acceleration processes at the deeper part of the seismogenic zone. Earth Planets Space 56, 1087–1093.
Shigematsu, N., 1999. Dynamic recrystallizatisation in deformed plagioclase during progressive shear deformation. Tectonophysics 305, 437–452.
Shigematsu, N., Tanaka, H., 2000. Dislocation creep of fine-grained recrystallized plagioclase under low-temperature conditions. Journal of Structural Geology 22, 65–79.
Shigematsu, N., Yamagishi, H., 2002. Quartz microstructures and deformation conditions in the Hatagawa shear zone, north-eastern Japan. The Island Arc 11, 45–60.

Shigematsu, N., Fujimoto, K., Ohtani, T., Goto, K., 2004. Ductile fracture of fine-grained plagioclase in the brittle-plastic transition regime: implication for earthquake source nucleation. Earth and Planetary Science Letters 222, 1007–1022.

Shimamoto, T., 1989. The origin of S–C mylonite and new fault zone model. Journal of Structural Geology 11, 51–64.

Sibson, R.H., 1982. Fault zone models, heat flow, and the depth distribution of earthquakes in the continental crust of the United States. Bulletin of the Seismological Society of America 72, 151–163.

Sibson, R.H., 1984. Roughness at the base of the seismogenic zone: contributing factors. Journal of Geophysical Research 89B, 5791–5799.

Simpson, C., 1985. Deformation of granitic rocks across the brittle-ductile transition. Journal of Structural Geology 7, 503–511.

Simpson, C., Wintsch, R.P., 1989. Evidence for deformation-induced K-feldspar replacement by myrmekite. Journal of Metamorphic Geology 7, 261–275.

Stewart, M., Holdsworth, R.E., Strachan, R.A., 2000. Deformation processes and weakening mechanisms within the frictional-viscous transition zone of major crustal-scale faults: insights from the Great Glen Fault Zone, Scotland. Journal of Structural Geology 22, 543–560.

Takagi, H., Goto, K., Shigematsu, N., 2000. Ultramylonite bands derived from cataclasite and pseudotachylyte in granites, northeast Japan. Journal of Structural Geology 22, 1325–1339.

Tomita, T., Ohtani, T., Shigematsu, N., Tanaka, H., Fujimoto, K., Kobayashi, Y., Miyashita, Y., Omura, K., 2002. Development of the Hatagawa Fault Zone clarified by geological and geochronological studies. Earth Planets Space 54, 1095–1102.

Tsurumi, J., Hosonuma, H., Kanagawa, K., 2003. Strain localizatisation due to a positive feedback deformation and myrmekite-forming reaction in granite and aplite mylonites along the Hatagawa Shear Zone of NE Japan. Journal of Structural Geology 25, 557–574.

Tullis, J., Yund, R.A., 1985. Dynamic recrystallizatisation of feldspar: a mechanism for ductile shear zone formation. Geology 13, 238–241.

Tullis, J., Yund, R.A., 1987. Transition from cataclastic flow to dislocation creep of feldspar: Mechanisms and microstructures. Geology 15, 606–609.

USGS Staff, 1990. The Loma Prieta, California, earthquake: an anticipated event. Science 247, 286–293.

Vernon, R.H., 1992. Question about myrmekite in deformed rocks. Journal of Structural Geology 13, 979–985.

Watanabe, I., Sotozaki, Y., Gorai, M., 1953. Geology of the northeastern border district of northern Abukuma Plateau. Science Report of the Tokyo Education University 2. 69-78. (in Japanese with English abstract.

White, S., 1976. The effect of strain on the microstructures, fabrics, and deformation mechanisms in quartzites. Philosophical Transactions of Royal Society of London A283, 69–86.

Whitney, J., Stormer, J.C., 1977. The distribution of $NaAlSi_3O_8$ between coexisting microcline and plagioclase and its effect on geothermometric calculations. American Mineralogist 62, 687–691.

Yund, R.A., 1983. Diffusion in feldspars. In: Wenk, P.H. (Ed.), Review in Mineralogy: Feldspar Mineralogy. The Mineralogical Society of America, Washington, DC, pp. 203–222.

Yund, R.A., Tullis, J., 1983. Subsolidus phase relations in the alkali feldspars with emphasis on coherent phases. In: Wenk, P.H. (Ed.), Review in Mineralogy: Feldspar Mineralogy. The Mineralogical Society of America, Washington, DC, pp. 141–176.

Yund, R.A., Tullis, J., 1991. Compositional changes of minerals associated with dynamic recrystallizatisation. Contributions to Mineralogy and Petrology 108, 346–355.

Zhao, D., Negishi, H., 1997. The 1995 Kobe earthquake: Seismic image of the source zone and its implications for the rupture nucleation. Journal of Geophysical Research 103B, 9967–9986.